

Supporting information for: “Origin of internal friction in disordered proteins depends on solvent quality”

Wenwei Zheng, Hagen Hofmann, Benjamin Schuler and Robert B. Best

Supplementary Figures.

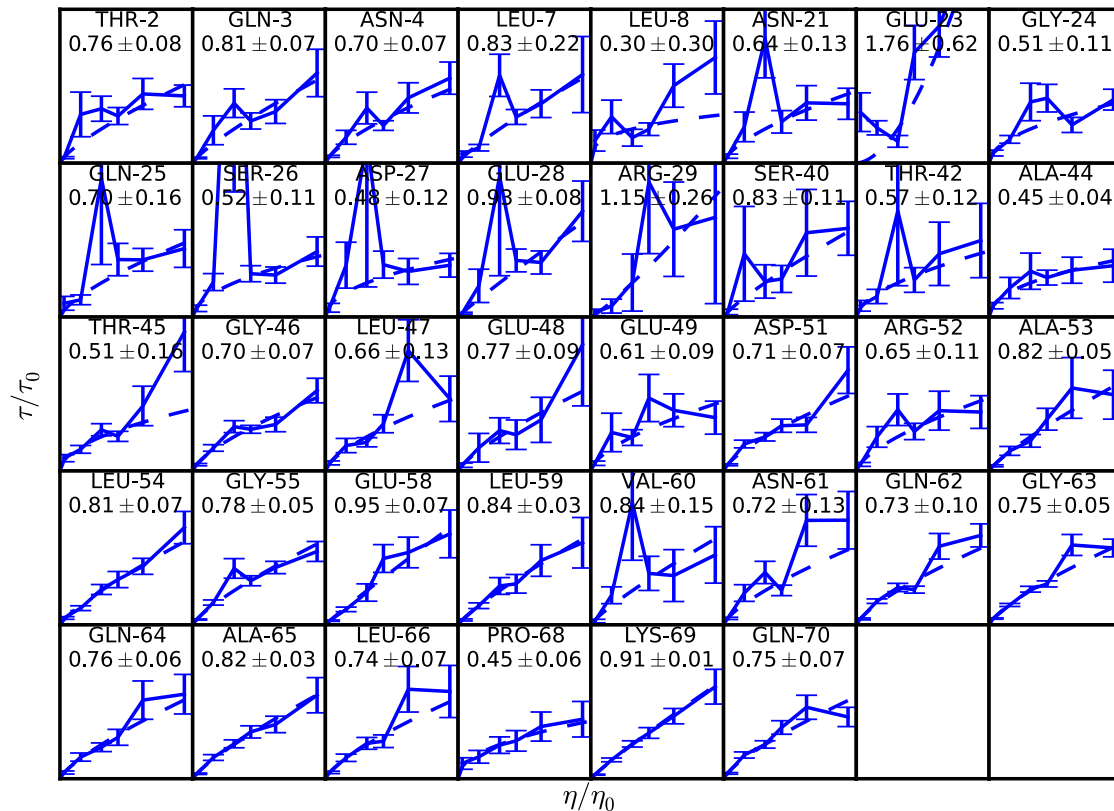


Figure S1. Internal friction on dihedral relaxation of ACTR. The title in each panel shows the residue index, name and the power-law fitting exponent β . Only the residues with more than 5 dihedral flipping events in the simulation are shown.

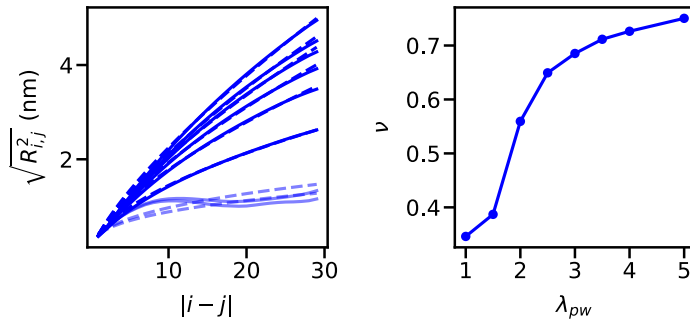


Figure S2. The length scaling exponent from fitting distances as a function of the sequence separation $\sqrt{R^2_{i,j}} = bN^\nu$. We determined both the prefactor b and the scaling exponent ν by globally fitting all the data with $\lambda_{pw} \geq 2.0$. We obtain the prefactor $b = 0.40$ nm for the coarse-grained homo-polypeptide model, which is expected to be different from the prefactor of a typical disordered protein (~ 0.55 nm)¹.

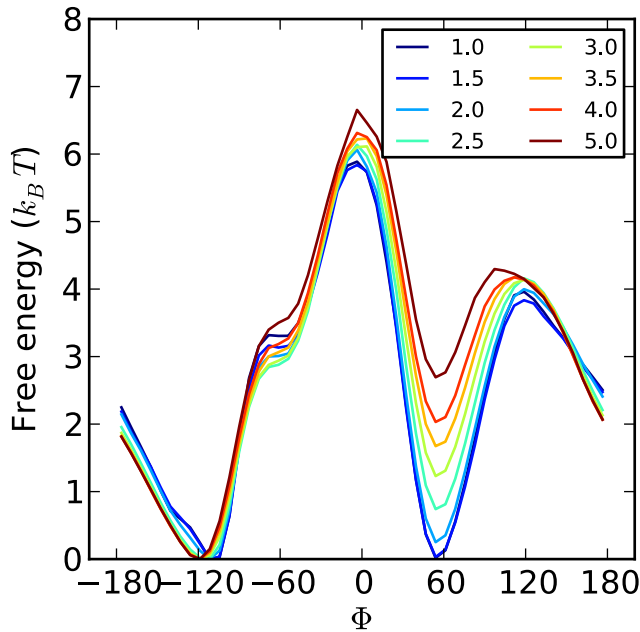


Figure S3. Free energy as a function of the dihedral angles in the coarse-grained simulations. The legend shows the scaling factor λ_{pw} of the pair interactions between the peptide and water.

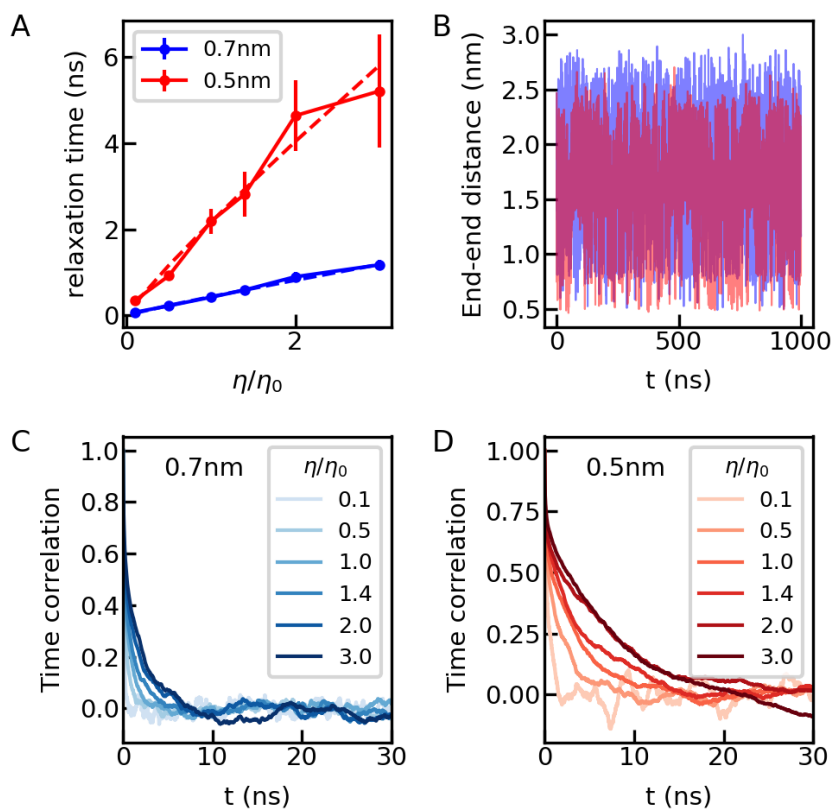


Figure S4. Relaxation time and time correlation function of end-end distance for the R_g -restrained simulations. A) The relaxation time of end-end distance for the R_g -restraint simulation with different targeted R_g . Legend shows the targeted R_g . B) Time series of end-end distances from the simulation trajectory of normal solvent viscosity, with color code the same as A). C and D) Time correlation function of end-end distance with different targeted R_g . Legend shows the solvent viscosity.

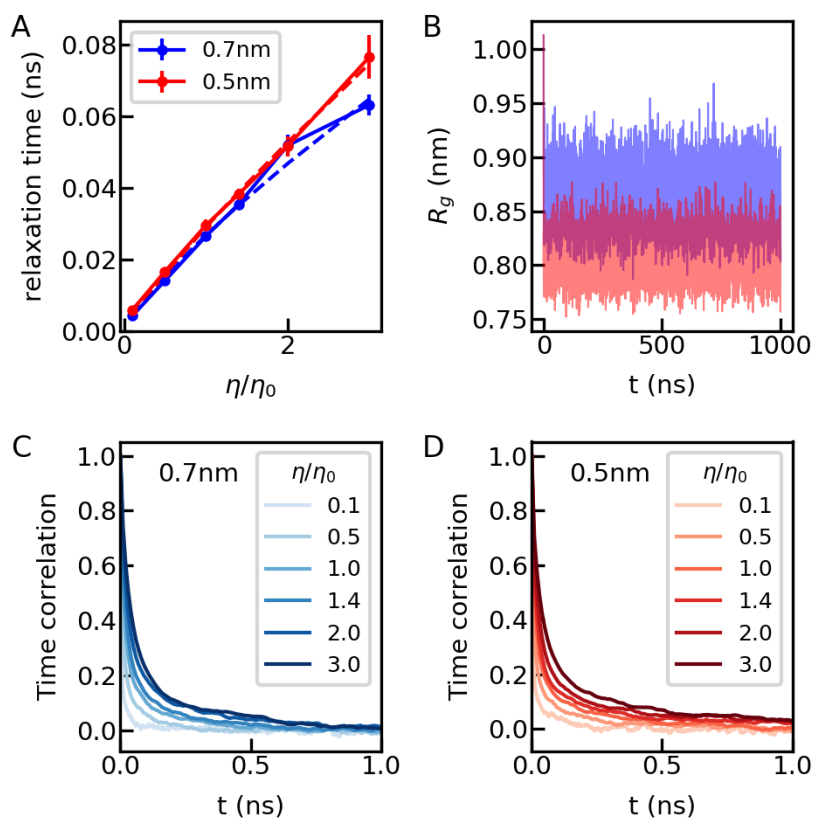


Figure S5. Relaxation time and time correlation function of R_g for the R_g -restrained simulations. A) The relaxation time of R_g for the R_g -restrained simulation with different targeted R_g . Legend shows the targeted R_g . B) Time series of R_g from the simulation trajectory of normal solvent viscosity, with color code as in A). C and D) Time correlation function of R_g with different targeted R_g . Legend shows the solvent viscosity.

Supplementary Tables.

Table S1. The scaling of water mass, the relative viscosity to water and the corresponding time step used in molecular dynamics simulations. The mass and viscosity of normal water are referred to by m_0 and η_0 , respectively.

| m/m_0 | η/η_0 | Time step (fs) |
|---------|---------------|----------------|
| 0.01 | 0.1 | 0.2 |
| 0.25 | 0.5 | 1 |
| 1 | 1 | 2 |
| 2 | 1.4 | 2 |
| 4 | 2 | 2 |
| 9 | 3 | 2 |

Table S2. R_g of ACTR. Estimates of radius of gyration of ACTR from simulation (present work) and several experimental sources. In brackets after the R_g value, we give the method used to analyze the experimental data, with “Guinier”, Guinier analysis², “Ensemble”, ensemble fitting³, SAW- ν , self-avoiding walking with adjustable scaling exponent⁴, and “Extended”, extended Guinier analysis with empirical fourth-order scattering vector term⁵. * indicates cases with small variations of chain length; the R_g values for these cases have been rescaled to a chain length of 71 using the corresponding scaling exponent by $R_{g,scaled} = R_g \cdot \left(\frac{71-1}{N-1}\right)^\nu$.

| Source | Method | Temperature (K) | Number of residues | R_g (nm) |
|-------------------|------------------------------------|-----------------|--------------------|---|
| Current | Simulation (Fig. 1F) | 295 | 71 | 2.23 ± 0.10 |
| Ref. ⁶ | SAXS | 278 | 71 | 2.63 (Guinier) |
| | | 318 | 71 | 2.39 (Guinier) |
| Ref. ³ | FRET | 298 | 75* | 2.33 ± 0.08 (Ensemble) 2.36 ± 0.06 (SAW- ν) |
| | SAXS (0.58M Urea) (0.32M GdmCl) | 298 | 79* | 2.34 ± 0.04 (Extended) 2.35 ± 0.03 (Extended) |
| | Simulation | 298 | 79* | 2.22 ± 0.21 |
| Ref. ⁷ | FRET | 295 | 75* | 2.47 ± 0.06 (SAW- ν) |

Table S3. Internal friction of ACTR.

| Method | β | $\alpha = \tau_0/\tau[\eta_0]$ | τ_0 (ns) |
|------------------------------|-------------|--------------------------------|---------------|
| Experiment | 0.75 (0.02) | 0.39 (0.05) | 64 (9) |
| Simulation | 0.64 (0.13) | 0.18 (0.16) | 32 (8) |
| Compact, dihedral restraint | 0.41 (0.29) | 0.56 (0.45) | 7.4 (1.6) |
| Extended, dihedral restraint | 1.04 (0.17) | -0.07 (0.15) | 5.2 (2.0) |

Table S4. Internal friction from the end-end distance relaxation time of the coarse-grained simulations.

| λ_{pw} | β | $\alpha = \tau_0/\tau[\eta_0]$ | τ_0 (ns) |
|----------------|-------------|--------------------------------|---------------|
| 1.0 | 0.52 (0.09) | 0.53 (0.17) | 2.10 (0.67) |
| 1.5 | 0.71 (0.17) | 0.32 (0.16) | 0.48 (0.02) |
| 2.0 | 0.75 (0.13) | 0.27 (0.21) | 0.38 (0.03) |
| 2.5 | 0.95 (0.03) | 0.07 (0.03) | 0.25 (0.03) |
| 3.0 | 0.92 (0.03) | 0.04 (0.02) | 0.30 (0.02) |
| 3.5 | 1.03 (0.05) | 0.003 (0.057) | 0.38 (0.02) |
| 4.0 | 1.00 (0.03) | 0.009 (0.035) | 0.44 (0.03) |
| 5.0 | 0.96 (0.01) | 0.03 (0.02) | 0.45 (0.02) |

Table S5. Internal friction when increasing dihedral barriers in the coarse-grained simulations.

| Added barrier (k _B T) | β | $\alpha = \tau_0/\tau[\eta_0]$ | τ_0 (ns) |
|----------------------------------|-------------|--------------------------------|---------------|
| 0 | 0.92 (0.03) | 0.04 (0.02) | 0.30 (0.02) |
| 2 | 1.09 (0.07) | -0.01 (0.10) | 0.35 (0.02) |
| 4 | 0.90 (0.03) | 0.09 (0.05) | 0.44 (0.05) |
| 6 | 0.53 (0.09) | 0.51 (0.19) | 0.76 (0.10) |

Table S6. Internal friction when introducing harmonic constraint on the dihedral angles (β_{freeze}) or introducing potential energy function to compensate dihedral barriers (β_{remove}) in the polypeptide simulation. $\lambda_{pw}=1.5$ corresponds to a compact state whereas $\lambda=2.0$ an expanded state.

| λ | $\beta_{original}$ | β_{freeze} | β_{remove} |
|-----------|--------------------|------------------|------------------|
| 1.5 | 0.71 (0.17) | 0.88 (0.04) | 0.58 (0.06) |
| 2.0 | 0.75 (0.13) | 0.98 (0.02) | 0.98 (0.08) |

Table S7. Internal friction when introducing harmonic constraint on the R_g in the polypeptide simulation. $\lambda_{pw}=5.0$ for these simulations.

| $R_{g-original}$ | Targeted R_g (nm) | $R_{g-restraint}$ (nm) | $\beta_{original}$ | $\beta_{restraint}$ | $\tau_{0,restraint}$ (ns) |
|------------------|---------------------|------------------------|--------------------|---------------------|---------------------------|
| 1.70 | 0.50 | 0.81 | 0.96 (0.01) | 0.90 (0.11) | 0.42 (0.02) |
| 1.70 | 0.70 | 0.86 | 0.96 (0.01) | 0.92 (0.04) | 2.18 (0.29) |

References.

1. Hofmann, H.; Soranno, A.; Borgia, A.; Gast, K.; Nettels, D.; Schuler, B., Polymer scaling laws of unfolded and intrinsically disordered proteins quantified with single-molecule spectroscopy. *Proc Natl Acad Sci USA* **2012**, *109* (40), 16155-16160.
2. Guinier, A., La diffraction des rayons x aux tres petits angles: applications a l'etude de phenomenes ultramicroscopiques. *Ann. Phys.* **1939**, *12*, 161-237.
3. Borgia, A.; Zheng, W.; Buholzer, K.; Borgia, M. B.; Schuler, A.; Hofmann, H.; Soranno, A.; Nettels, D.; Gast, K.; Grishaev, A.; Best, R. B.; Schuler, B., Consistent View of Polypeptide Chain Expansion in Chemical Denaturants from Multiple Experimental Methods. *J Am Chem Soc* **2016**, *138* (36), 11714-26.
4. Zheng, W.; Zerze, G. H.; Borgia, A.; Mittal, J.; Schuler, B.; Best, R. B., Inferring properties of disordered chains from FRET transfer efficiencies. *J Chem Phys* **2018**, *148* (12).
5. Zheng, W.; Best, R. B., An Extended Guinier Analysis for Intrinsically Disordered Proteins. *J Mol Biol* **2018**, *430* (16), 2540-2553.
6. Kjaergaard, M.; Nørholm, A.-B.; Hendus-Altenburger, R.; Pedersen, S. F.; Poulsen, F. M.; Kragelund, B. B., Temperature-dependent structural changes in intrinsically disordered proteins: formation of alpha-helices or loss of polyproline II? *Protein Sci* **2010**, *19* (8), 1555-1564.
7. Soranno, A.; Zosel, F.; Hofmann, H., Internal friction in an intrinsically disordered protein: comparing Rouse-like models with experiments. *J. Chem. Phys* **2018**, *148*, 123326.